

The t - J model: From light to heavy doping

A. Sherman

Institute of Physics, University of Tartu, Riia 142, 51014 Tartu, Estonia

(Dated: November 14, 2018)

The regions of hole concentrations $0 \leq x \lesssim 0.3$ and temperatures $0.005|t| \leq T \leq 0.02|t|$ are studied in the t - J model of Cu-O planes of perovskite high- T_c superconductors. For this purpose self-energy equations for hole and spin Green's functions are derived using Mori's projection operator technique and these equations are self-consistently solved. The calculated hole band transforms radically at $x \approx 0.08$. A narrow low-concentration band with minima near $(\pm\frac{\pi}{2}, \pm\frac{\pi}{2})$ is converted to a band resembling the case of weak electron correlations, with the minimum at (π, π) or $(0, 0)$. The hole Fermi surface is respectively changed from small ellipses at $(\pm\frac{\pi}{2}, \pm\frac{\pi}{2})$ to a large rhombus centered at (π, π) or $(0, 0)$. The decrease of the magnetic susceptibility at the antiferromagnetic wave vector and spin correlations with doping is determined by the growth of the frequency of spin excitations at this momentum. The shape of the frequency dependence of the susceptibility depends heavily on the hole damping and varies from a broad feature similar to that observed in $\text{La}_{2-x}\text{Sr}_x\text{CuO}_4$ to a pronounced maximum which resembles the normal-state resonance peak in $\text{YBa}_2\text{Cu}_3\text{O}_{7-y}$.

PACS numbers: 71.10.Fd, 74.25.Ha, 74.25.Jb

I. INTRODUCTION

The two-dimensional t - J model was proposed by Anderson¹ for the description of strong electron correlations in Cu-O planes of perovskite high- T_c superconductors. In Ref. 2 the similarity of the low-energy part of its spectrum with the spectrum of the realistic three-band Hubbard model was demonstrated. Nowadays the t - J model is one of the most frequently used models for the interpretation of experimental results in cuprates (for a review, see Ref. 3). Different numerical and analytical methods were used for the investigation of the model. Among these methods are the exact diagonalization of small clusters,^{4,5} Monte Carlo simulations,⁶ density matrix renormalization group calculations,⁷ spin-wave^{8,9} and mean-field slave-boson approximations.¹⁰ In spite of the considerable progress made towards the understanding of the properties of the model, the basic issues of its behavior in going from light to heavy hole doping have not yet been completely resolved. In particular, there is still no clear knowledge of how the narrow spin-polaron band inherent in light doping is converted to a wide band observed in photoemission of optimally and overdoped crystals.¹¹ The investigation of the variation of the magnetic susceptibility with the hole doping, temperature and the damping of excitations is also of great importance in view of a great body of data obtained in inelastic neutron scattering.¹²

Aiming at a description for the wide range of hole concentrations in this paper we use the method¹³ based on Mori's projection operator technique.¹⁴ The method allows one to derive self-energy equations for Green's functions constructed from Hubbard operators without recourse to the intricate diagrammatic technique. These equations retain the rotation symmetry of spin components inherent in the Hamiltonian and do not imply any preset magnetic ordering. In contrast to Ref. 13, where this approach was implemented for the spin subsystem

only, in this work we use it also for the hole subsystem.

The obtained equations were self-consistently solved in a 20×20 lattice for the ranges of hole concentrations $0 \leq x \lesssim 0.3$ and temperatures $0.005|t| \leq T \leq 0.02|t|$ where t is the hopping constant of the t - J model. In cuprates this concentration range covers the regions from light to heavy doping. The ratios of the exchange J and hopping parameters of the model $J/|t| = 0.4$ and $J/|t| = 0.2$ were used. Such ratios correspond to hole-doped cuprates.¹⁵ For $|t| \approx 0.5$ eV the boundaries of the above temperature range correspond approximately to 30 K and 120 K.

Obtained results indicate that the hole band transforms radically at $x \approx 0.08$. A narrow low-concentration band with minima near $(\pm\frac{\pi}{2}, \pm\frac{\pi}{2})$ is converted to a band resembling in its shape the case of weak electron correlations, with the minimum at (π, π) or at $(0, 0)$ in dependence on the sign of t . The hole Fermi surface is respectively changed from small elliptical pockets at $(\pm\frac{\pi}{2}, \pm\frac{\pi}{2})$ to a large rhombus centered at (π, π) or $(0, 0)$. With increasing x the maximum in the imaginary part of the magnetic susceptibility χ'' at the antiferromagnetic wave vector $\mathbf{Q} = (\pi, \pi)$ loses its intensity and shifts to higher frequencies. This behavior is mainly connected with the growth of the frequency of spin excitations at \mathbf{Q} and is consistent with experimental data. The shape of the frequency dependence of $\chi''(\mathbf{Q})$ depends heavily on the hole damping and varies from a broad feature similar to that observed¹⁶ in $\text{La}_{2-x}\text{Sr}_x\text{CuO}_4$ to a pronounced maximum which is analogous to the normal-state resonance peak¹⁷ in $\text{YBa}_2\text{Cu}_3\text{O}_{7-y}$.

II. MAIN FORMULAS

The Hamiltonian of the two-dimensional t - J model reads

$$H = \sum_{\mathbf{nm}} t_{\mathbf{nm}} a_{\mathbf{n}\sigma}^\dagger a_{\mathbf{m}\sigma} + \frac{1}{2} \sum_{\mathbf{nm}} J_{\mathbf{nm}} (s_{\mathbf{n}}^z s_{\mathbf{m}}^z + s_{\mathbf{n}}^{+1} s_{\mathbf{m}}^{-1}), \quad (1)$$

where $a_{\mathbf{n}\sigma} = |\mathbf{n}\sigma\rangle\langle\mathbf{n}0|$ is the hole annihilation operator, \mathbf{n} and \mathbf{m} label sites of the square lattice, $\sigma = \pm 1$ is the spin projection, $|\mathbf{n}\sigma\rangle$ and $|\mathbf{n}0\rangle$ are site states corresponding to the absence and presence of a hole on the site. These states may be considered as linear combinations of the products of the $3d_{x^2-y^2}$ copper and $2p_\sigma$ oxygen orbitals of the extended Hubbard model.¹⁸ We take into account nearest neighbor interactions only, $t_{\mathbf{nm}} = t \sum_{\mathbf{a}} \delta_{\mathbf{n},\mathbf{m}+\mathbf{a}}$ and $J_{\mathbf{nm}} = J \sum_{\mathbf{a}} \delta_{\mathbf{n},\mathbf{m}+\mathbf{a}}$ where the four vectors \mathbf{a} connect nearest neighbor sites. The spin- $\frac{1}{2}$ operators can be written as $s_{\mathbf{n}}^z = \frac{1}{2} \sum_{\sigma} \sigma | \mathbf{n}\sigma \rangle \langle \mathbf{n}\sigma |$ and $s_{\mathbf{n}}^\sigma = | \mathbf{n}\sigma \rangle \langle \mathbf{n}, -\sigma |$.

Properties of the model are determined from the hole and spin retarded Green's functions

$$\begin{aligned} G(\mathbf{k}t) &= -i\theta(t) \langle \{a_{\mathbf{k}\sigma}(t), a_{\mathbf{k}\sigma}^\dagger\} \rangle, \\ D(\mathbf{k}t) &= -i\theta(t) \langle [s_{\mathbf{k}}^z(t), s_{-\mathbf{k}}^z] \rangle, \end{aligned} \quad (2)$$

where $a_{\mathbf{k}\sigma}$ and $s_{\mathbf{k}}^z$ are the Fourier transforms of the respective site operators, operator time dependencies and averaging are defined with the Hamiltonian $\mathcal{H} = H - \mu \sum_{\mathbf{n}} a_{\mathbf{n}\sigma}^\dagger a_{\mathbf{n}\sigma}$ with the chemical potential μ . As mentioned, to obtain self-energy equations for these functions we used Mori's projection operator technique.^{13,14} In this approach the Fourier transform of Green's function $\langle\langle A_0 | A_0^\dagger \rangle\rangle$ is represented by the continued fraction

$$\langle\langle A_0 | A_0^\dagger \rangle\rangle = \frac{|A_0 \cdot A_0^\dagger|}{\omega - E_0 - \frac{V_0}{\omega - E_1 - \frac{V_1}{\ddots}}}. \quad (3)$$

The elements of the fraction E_i and V_i are determined from the recursive procedure

$$\begin{aligned} [A_n, H] &= E_n A_n + A_{n+1} + V_{n-1} A_{n-1}, \\ E_n &= |[A_n, H] \cdot A_n^\dagger| |A_n \cdot A_n^\dagger|^{-1}, \\ V_{n-1} &= |A_n \cdot A_n^\dagger| |A_{n-1} \cdot A_{n-1}^\dagger|^{-1}, \\ V_{-1} &= 0, \quad n = 0, 1, 2, \dots \end{aligned} \quad (4)$$

The operators A_i constructed in the course of this procedure form an orthogonal set, $|A_i \cdot A_j^\dagger| \propto \delta_{ij}$. In Eqs. (3) and (4) the definition of the inner product $|A_i \cdot A_j^\dagger|$ depends on the type of the considered Green's function. For example, for functions (2) these are $\langle\{A_i, A_j^\dagger\}\rangle$ and $\langle[A_i, A_j^\dagger]\rangle$, respectively. The method described by Eqs. (3) and (4) can be straightforwardly generalized

to the case of many-component operators which is necessary, for example, to consider Green's functions for Nambu spinors in the superconducting state.¹³

The residual term of fraction (3) is the Fourier transform of the quantity

$$\mathcal{T} = |A_{nt} \cdot A_n^\dagger| |A_{n-1} \cdot A_{n-1}^\dagger|^{-1}, \quad (5)$$

where the time evolution of the operator A_n is determined by the equation

$$i \frac{d}{dt} A_{nt} = \prod_{k=0}^{n-1} (1 - P_k) [A_{nt}, \mathcal{H}], \quad A_{n,t=0} = A_n \quad (6)$$

with the projection operators P_n defined as $P_n Q = |Q \cdot A_n^\dagger| |A_n \cdot A_n^\dagger|^{-1} A_n$. The residual term \mathcal{T} is a many-particle Green's function which can be estimated by the decoupling. Following Ref. 19 the decoupling procedure may be somewhat improved by introducing the vertex correction α which is determined from the constraint of zero site magnetization

$$\langle s_{\mathbf{n}}^z \rangle = \frac{1}{2} (1 - x) - \langle s_{\mathbf{n}}^{-1} s_{\mathbf{n}}^{+1} \rangle = 0. \quad (7)$$

The spin Green's function obtained in this way reads¹³

$$\begin{aligned} D(\mathbf{k}\omega) &= \frac{4(\gamma_{\mathbf{k}} - 1)(JC_1 + tF_1)}{\omega^2 - \omega \text{Im}(\mathbf{k}\omega) - \omega_{\mathbf{k}}^2}, \\ \text{Im} \Pi(\mathbf{k}\omega) &= \frac{9\pi t^2 J^2 (1 - x)}{2N(\gamma_{\mathbf{k}} - 1)(JC_1 + tF_1)} \end{aligned} \quad (8)$$

$$\begin{aligned} &\times \sum_{\mathbf{k}'} (\gamma_{\mathbf{k}+\mathbf{k}'} - \gamma_{\mathbf{k}'})^2 \int_{-\infty}^{\infty} d\omega' A(\mathbf{k}'\omega') \\ &\times A(\mathbf{k} + \mathbf{k}', \omega + \omega') \frac{n_F(\omega + \omega') - n_F(\omega)}{\omega}, \end{aligned}$$

where $\gamma_{\mathbf{k}} = \frac{1}{2} [\cos(k_x) + \cos(k_y)]$, $C_1 = \langle s_{\mathbf{n}}^{+1} s_{\mathbf{n}+\mathbf{a}}^{-1} \rangle$ and $F_1 = \langle a_{\mathbf{n}}^\dagger a_{\mathbf{n}+\mathbf{a}} \rangle$ are the spin and hole correlations on neighboring sites which can be derived from the respective Green's functions,

$$\langle s_{\mathbf{n}}^{+1} s_{\mathbf{m}}^{-1} \rangle = \frac{2}{N} \sum_{\mathbf{k}} e^{i\mathbf{k}(\mathbf{n}-\mathbf{m})} \int_{-\infty}^{\infty} d\omega [1 + n_B(\omega)] B(\mathbf{k}\omega), \quad (9)$$

$$\langle a_{\mathbf{n}}^\dagger a_{\mathbf{m}} \rangle = \frac{1}{N} \sum_{\mathbf{k}} e^{i\mathbf{k}(\mathbf{n}-\mathbf{m})} \int_{-\infty}^{\infty} d\omega n_F(\omega) A(\mathbf{k}\omega),$$

$$\omega_{\mathbf{k}}^2 = 16J^2\alpha|C_1|(1 - \gamma_{\mathbf{k}})(\Delta + 1 + \gamma_{\mathbf{k}}), \quad (10)$$

is the square of the frequency of spin excitations with the parameter Δ describing the spin gap near \mathbf{Q} , N is the number of sites, $A(\mathbf{k}\omega) = -\pi^{-1} \text{Im} G(\mathbf{k}\omega)$ and $B(\mathbf{k}\omega) = -\pi^{-1} \text{Im} D(\mathbf{k}\omega)$ are the hole and spin spectral functions, $n_F(\omega) = [\exp(\omega/T) + 1]^{-1}$, $n_B(\omega) = [\exp(\omega/T) - 1]^{-1}$ with the temperature T . The real part of the self-energy

$\Pi(\mathbf{k}\omega)$ can be calculated from its imaginary part and the Kramers-Kronig relation. However, in the calculations $\text{Re } \Pi$ was neglected, since the gap parameter Δ and along with it the magnon frequencies near \mathbf{Q} were determined from the constraint (7). This momentum region plays the main role in the considered spectral and magnetic properties. As follows from earlier calculations,¹³ the vertex parameter α depends mainly on x and can be approximated as $\alpha = 1.802 - 0.802 \tanh(10x)$.

Two steps of the procedure (3), (4) can be also carried out for the hole Green's function. We find

$$\begin{aligned} \langle \{a_{\mathbf{k}\sigma}, a_{\mathbf{k}\sigma}^\dagger\} \rangle &= \frac{1}{2}(1+x) = \phi, \\ E_0 &= (4t\phi + 6tC_1\phi^{-1} - 3JF_1\phi^{-1})\gamma_{\mathbf{k}} \\ &\quad + 4tF_1\phi^{-1} - 3JC_1\phi^{-1} - \mu, \\ V_0 &= 24t^2C'_\mathbf{k} + 16t^2(3C_1 + \phi^2)\gamma_{\mathbf{k}} \\ &\quad + t^2 \left[\frac{1}{4}x(1-x) - 4C_1 \left(1 + \frac{3}{2}x \right) \phi^{-1} \right] \\ &\quad + 24t^2F_1\gamma_{\mathbf{k}} - 4t(3C_1\phi^{-1} + 2\phi)(E_0 + \mu)\gamma_{\mathbf{k}} \\ &\quad - 8tF_1(E_0 + \mu) + (E_0 + \mu)^2, \\ E_1 &\approx -\mu, \end{aligned} \quad (11)$$

where $x = N^{-1} \sum_{\mathbf{k}} \int_{-\infty}^{\infty} d\omega n_F(\omega) A(\mathbf{k}\omega)$ and $C'_\mathbf{k} = 2N^{-1} \sum_{\mathbf{k}'} \gamma_{\mathbf{k}-\mathbf{k}'}^2 \langle s_{\mathbf{k}'}^z s_{-\mathbf{k}'}^z \rangle$. If the continued fraction (3) is terminated at this stage, the hole spectrum is approximated by two poles which form two bands,

$$G(\mathbf{k}\omega) = \frac{\phi(\mu - \omega)}{(\tilde{E}_0^2 + V_0)^{1/2}} \left(\frac{1}{\omega - \varepsilon_{\mathbf{k},1} + \mu + i\eta} - \frac{1}{\omega - \varepsilon_{\mathbf{k},2} + \mu + i\eta} \right), \quad (12)$$

where

$$\begin{aligned} \tilde{E}_0 &= (4t\phi + 6tC_1\phi^{-1} - 3JF_1\phi^{-1})\gamma_{\mathbf{k}}, \\ \varepsilon_{\mathbf{k},j} &= \tilde{E}_0/2 \pm (\tilde{E}_0^2/4 + V_0)^{1/2}, \end{aligned} \quad (13)$$

and η is a damping of the hole states. In the framework of the t - J model this damping is connected with the hole-magnon scattering.¹³ However, in this work the damping is considered as a free parameter to take into account other possible damping processes. Such approach is motivated by the fact that the damping of spin excitations (8) depends heavily on the value of η and to investigate different shapes of the frequency dependence of the susceptibility η is considered as a variable parameter.

Thus, in the present work the calculation of the elements of the continued fraction E_i and V_i for the spin Green's function was carried out up to the second order: E_0 , V_0 and E_1 were calculated. Then the residual term of the continued fraction (the part of the fraction containing the third and higher order terms) which is represented by the many-particle Green's function (5) is approximated

by the decoupling. The same elements of the continued fraction were calculated for the hole Green's function [see Eq. (11)]. In this case the residual part of the continued fraction was omitted and the artificial damping η was added. The main argument for the above truncations of the continued fractions is based on the results obtained previously. In Ref. 19 the analogous truncation in the equations of motion with the decoupling improved by a vertex correction was successfully used for the description of spin excitations in the Heisenberg model. For the lightly doped t - J model this approximation was used in Ref. 13 and the results obtained were in good agreement with the exact diagonalization of small clusters. The two-pole approximation for the hole Green's function was shown to give a good description of the spin-polaron band for moderate $|t|/J$ in the spin-wave approach.⁸ In a more general perspective the used method is a version of the Lanczos algorithm. It is known from numerical methods that at a successful choice of the starting vector this algorithm gives good approximations for outermost eigenvalues and eigenvectors of a matrix already with few steps.

Equations (7)–(12) form a closed set which can be solved by iteration for given values of the chemical potential, temperature, hole damping and the sign of t .

III. EVOLUTION OF THE HOLE SPECTRUM

Results of our calculations for the lowest of the hole bands which crosses the Fermi level are shown in Figs. 1 and 2 for different values of the hole concentrations and the sign of t . Notice that for low hole concentrations the shape of the band is close to the shape of the spin-polaron band obtained in the spin-wave approximation^{3,8} and in the approach of Ref. 13. However, for the parameters chosen the bandwidth is half as much again the value found in the two mentioned approaches. This difference is a consequence of our two-pole approximation (12) for the hole Green's function. For small x the shape of the band depends only weakly on the sign of t . With increasing x the band changes rapidly and already for moderate concentrations its shapes for opposite signs of t differ essentially and resemble shapes of weakly correlated bands. As this takes place, the bandwidth grows and for $x \approx 0.3$ it is three times as much as the bandwidth for light doping.

The decrease of the temperature to $T = 0.005|t|$, of the hole damping to $\eta = 0.015|t|$ or the increase of the exchange constant to $J = 0.4|t|$ do not change qualitatively the evolution of the hole band with doping. For all these parameters the transformation of the hole band from the shape typical for strong correlations to that resembling the weakly correlated case occurs at $x \approx 0.08$. As this takes place, the respective Fermi surface, shown in the base planes in Figs. 1 and 2, changes its shape from small ellipses at $(\pm\frac{\pi}{2}, \pm\frac{\pi}{2})$ for small x to a large rhombus centered at (π, π) or $(0, 0)$ for large x . The van Hove sin-

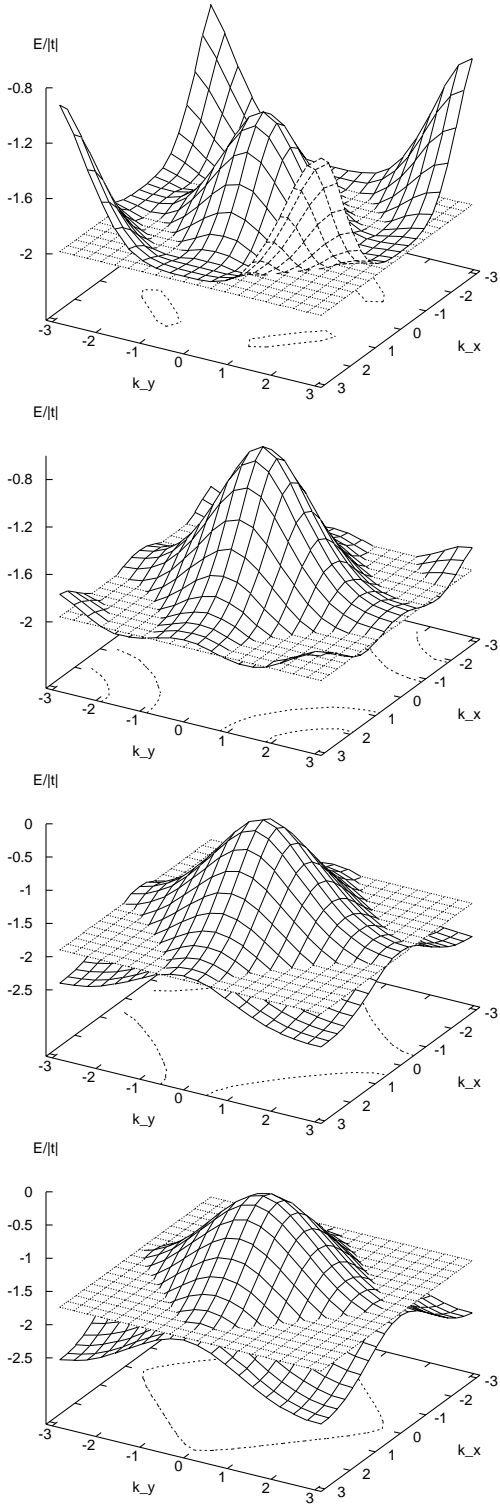


FIG. 1: The hole dispersion for $t > 0$, $J/t = 0.2$, $T = 0.02t$, $\eta = 0.05t$ and $x = 0.033, 0.076, 0.14$, and 0.18 (from top to bottom). Horizontal planes are the Fermi levels. The respective Fermi surfaces are shown in the base planes.

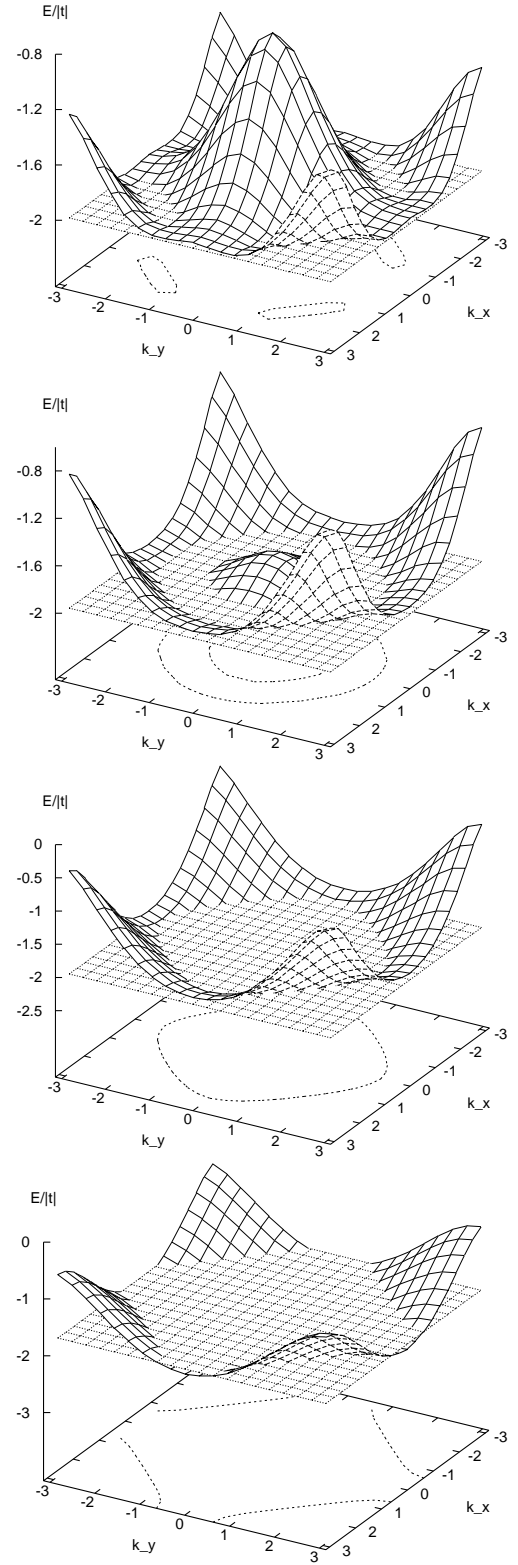


FIG. 2: The hole dispersion for $t < 0$, $J/|t| = 0.2$, $T = 0.02|t|$, $\eta = 0.05|t|$ and $x = 0.033, 0.076, 0.13$, and 0.2 (from top to bottom).

gularity of the hole band located at $(0, \pi)$ remains near the Fermi level in the wide range of hole concentrations $x \lesssim 0.2$.

The reason for the above transformation of the band shape is in the following. For small hole concentrations the hole dispersion is determined by the magnetic ordering which is close to the long-range antiferromagnetic order. In this case the elementary cell in the direct space is doubled due to the opposite alignment of spins on neighboring sites. Hence the Brillouin zone becomes half the value of the paramagnetic zone and the points $(0, 0)$ and (π, π) become equivalent. In particular, this means that the hole dispersion is approximately invariant with respect to the substitution $\mathbf{k} \rightarrow \mathbf{k} + \mathbf{Q}$, as seen in the upper parts of Fig. 1 and 2. Mathematically this corresponds to the case when $|\tilde{E}_0| \ll V_0$ in $\varepsilon_{\mathbf{k},j}$ in Eq. (13). With increasing x the spin correlation length ξ is decreased. When¹³ $\xi = \frac{1}{2}a\Delta^{-1/2}$ becomes comparable to a few lattice spacings a the above arguments cease to work. In this case the hole dispersion is determined by \tilde{E}_0 which becomes larger than V_0 and the band acquires the shape which is similar to the case of weak correlations. However, even for $x = 0.25$ the bandwidth is much smaller than $8|t|$, the bandwidth in the latter case (see the lower parts of Fig. 1 and 2). Thus, even in the overdoped case the corrections due to electron correlations are essential. The above transformation is not connected with some sharp transition in the magnetic subsystem. The decrease of the spin correlation length with x is continuous.

The analogous transformation of the hole band is expected also in the more complicated and flexible t - t' - t'' - J model which is frequently used for the interpretation of experimental results in cuprates.^{3,11} The respective value of the hole concentration is supposed to be close to 0.08. This assumption is based on the fact that the transformation occurs when the correlation length approaches a few lattice spacings. The correlation length derived from neutron scattering experiments¹² in cuprates acquires this value near the mentioned concentration.

In the considered two-pole approximation only one hole band crosses the Fermi level. In contrast to this the calculations based on the spin-wave approximation⁸ and on the approach of Ref. 13, which are supposed to be more accurate for low hole concentrations, show that for $x > 0.05$ there are two bands crossing the Fermi level. One of these bands is the spin-polaron band which corresponds to a pronounced peak in the hole spectral function and has the dispersion similar to that shown in upper parts of Figs. 1 and 2. The second band has a much weaker and broader peak in $A(\mathbf{k}\omega)$ and therefore its contribution to the lower band of the two-pole approximation can be neglected. Thus, the lower hole band which cross the Fermi level corresponds to the feature with the highest peak intensity in the hole spectrum – the spin-polaron band. The upper band corresponds to “everything else” in the hole spectrum. From previous considerations (see Refs. 3,8,13 and references therein) it is known that in $A(\mathbf{k}\omega)$ for low x several weaker and

broader maxima are located above the spin-polaron peak. These maxima merge into one broad maximum at larger concentrations. The upper band of the two-pole approximation gives a rough description for these peculiarities of the hole spectrum. Since states near the Fermi level are of main interest and this approximation gives a satisfactory description for these states, it is used in the present work.

It is worth noting that the used two-pole approximation for the hole Green’s function gives satisfactory results not only in the limit of small x but also in the limit $x \rightarrow 1$. Indeed, in this limit $V_0 \rightarrow 0$, $E_0 \approx 4t\gamma_{\mathbf{k}} - \mu$ and $G(\mathbf{k}\omega) = (\omega - 4t\gamma_{\mathbf{k}} + \mu)^{-1}$. However, the two-pole approximation becomes inapplicable in the intermediate region for $x > 0.3$ when the chemical potential falls into the gap between two bands.

IV. MAGNETIC SUSCEPTIBILITY

The imaginary part of the magnetic susceptibility is given by the equation

$$\begin{aligned} \chi''(\mathbf{k}\omega) &= 4\pi\mu_B^2 B(\mathbf{k}\omega) \\ &= \frac{16\mu_B^2(1 - \gamma_{\mathbf{k}})(JC_1 + tF_1)\omega\text{Im}\Pi}{(\omega^2 - \omega\text{Re}\Pi - \omega_{\mathbf{k}}^2)^2 + (\omega\text{Im}\Pi)^2}, \end{aligned} \quad (14)$$

where μ_B is the Bohr magneton. For the considered hole concentrations the hole contribution to the susceptibility is much smaller than the spin contribution.⁸ Up to $x \approx 0.13$ the momentum dependence of χ'' is strongly peaked at \mathbf{Q} (the use of a comparatively small 20×20 lattice does not allow us to describe the incommensurability of the magnetic response – the low-density inverse space and the frequency independent damping η produce a minimum in the spin-excitation damping $\text{Im}\Pi(\mathbf{k})$ at $\mathbf{k} = \mathbf{Q}$ which is too shallow to give rise to incommensurability^{13,20}). The calculated frequency dependencies of the susceptibility at this momentum are shown in Fig. 3. In $\text{La}_{1.86}\text{Sr}_{0.14}\text{CuO}_4$ the susceptibility is peaked at incommensurate momenta $\mathbf{k} = (\pi \pm 2\pi\delta, \pi), (\pi, \pi \pm 2\pi\delta)$. The experimental susceptibility measured¹⁶ at one of these momenta is also shown in Fig. 3a. To demonstrate the similarity of the experimental and calculated dependencies the former was increased by approximately 2.5 times (the difference in the peak amplitudes is apparently connected with the splitting of the commensurate peak into 4 incommensurate maxima). As mentioned above, for the comparison with experiment we set $t = 0.5$ eV, thus the temperatures $T = 0.005t$ and $T = 0.02t$ in the figure correspond to 29 K and 116 K, respectively.

As seen from Fig 3a, the calculated frequency dependencies are close to those observed in $\text{La}_{1.86}\text{Sr}_{0.14}\text{CuO}_4$ for both temperatures. For $T = 0.005t$ the susceptibility has a broad maximum at $\omega \approx 7$ meV. This maximum is not connected with the resonance denominator in Eq. (14), because for the parameters chosen spin excitations near \mathbf{Q} are overdamped – their dampings are larger

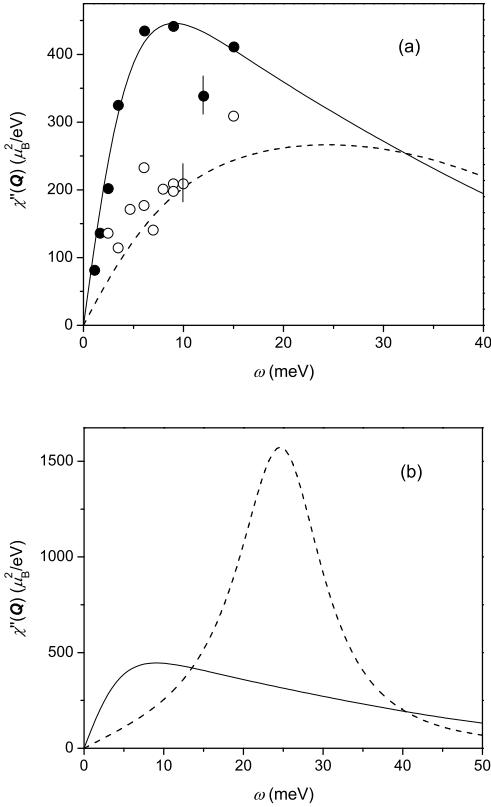


FIG. 3: The frequency dependence of the imaginary part of the susceptibility. (a) The solid line corresponds to $J = 0.2t$, $t > 0$, $T = 0.005t$, $\eta = 0.05t$ and $x \approx 0.1$. The dashed line are for $T = 0.02t$ and the same other parameters. Symbols are experimental results¹⁶ in $\text{La}_{1.86}\text{Sr}_{0.14}\text{CuO}_4$ at $T = 35$ K (filled circles) and $T = 80$ K (open circles). Vertical bars show experimental errors. The calculated susceptibility is given for $\mathbf{k} = \mathbf{Q}$, the experimental data are for the wave vector of the incommensurate peak. (b) The solid line is the same as in part (a). The dashed line is calculated for $\eta = 0.015t$, other parameters are the same as for the solid line.

than their frequencies. A completely different situation occurs with the decreased hole damping. The dampings of spin excitations decrease also, the excitations cease to be overdamped and the shape of the susceptibility is determined by the resonance denominator in Eq. (14). In this case χ'' has a pronounced maximum at $\omega \approx \omega_{\mathbf{k}}$, as seen in Fig. 3b. The shape of the dashed curve in this figure is similar to the resonance peak observed in the normal state of the underdoped $\text{YBa}_2\text{Cu}_3\text{O}_{7-y}$.¹⁷ Thus, we suppose that the dissimilarity of the frequency dependences of the susceptibility in this crystal and in $\text{La}_{2-x}\text{Sr}_x\text{CuO}_4$ is connected with different values of the damping of spin excitations. One of the possible reasons for this difference is the diverse values of the hole damping.

The evolution of $\chi''(\mathbf{Q}\omega)$ with the increase of the hole concentration is shown in Fig. 4. For the damping chosen all 3 curves have pronounced maxima, however also for a larger damping, when spin excitations are overdamped,

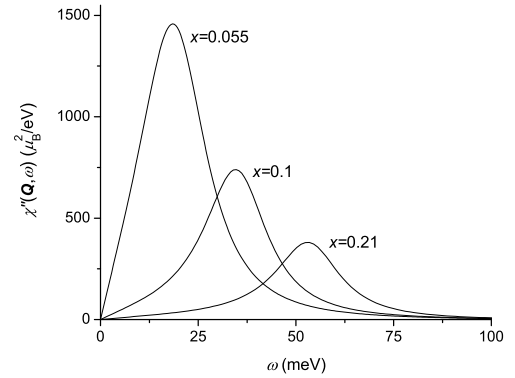


FIG. 4: The susceptibility at the antiferromagnetic wave vector for the 3 hole concentrations indicated near the curves. Other parameters are $J = 0.2t$, $T = 0.02t$, $\eta = 0.02t$ and $t > 0$.

the behavior of the susceptibility is similar to that shown in the figure. With growing x the frequency of the maximum increases and its amplitude decreases. This behavior points to the increase of the spin excitation frequency $\omega_{\mathbf{Q}}$ with the hole concentration. It can be shown¹⁹ that the value of this frequency is directly connected with the magnetic correlation length ξ . From the obtained results it follows that for low hole concentrations and temperatures $\xi \approx ax^{-1/2}$ where a is the intersite distance. An analogous relation has been derived from experimental data in $\text{La}_{2-x}\text{Sr}_x\text{CuO}_4$.²¹ The peak amplitudes of the susceptibility decreases rapidly with increasing x for $x \lesssim 0.11$ and then flattens out. The rapid decrease can be related to the transformation of the hole band discussed in the previous section. The qualitative behavior of the peak amplitude is not changed with the increase of the exchange constant to $J = 0.4t$, with the decrease of the temperature to $T = 0.005t$ or with the change of the sign of t . The qualitatively similar behavior of the susceptibility is observed¹⁷ in the normal-state $\text{YBa}_2\text{Cu}_3\text{O}_{7-y}$. However, in experiment the decrease of the peak intensity is somewhat slower for small x and the maximum of the susceptibility is smeared out for $x > 0.16$. These features depend strongly on the damping of spin excitations which is described only crudely in the used two-pole approximation.

The decrease of the susceptibility at the antiferromagnetic wave vector with doping is reflected in the weakening of spin correlations $C_1 = \langle s_1^{+1} s_0^{-1} \rangle$. These correlations are shown in Fig. 5 where the components of the vector \mathbf{l} are designated as n and m . In this figure the correlations obtained⁵ by exact diagonalization in a 4×4 lattice for $J = 0.4t$ and $T = 0$ are also shown. The difference between the two sets of data is connected with the influence of finite-size effects in the latter data and with the known issue of the method used in our calculations which somewhat underestimates the correlations.^{13,19} The correlations change only slightly with the change of the sign of t and with the variation of J and T in the considered

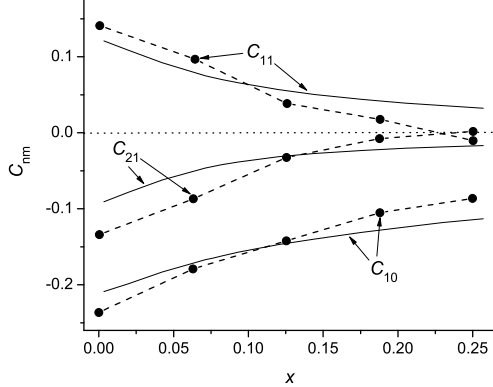


FIG. 5: The spin correlations $C_1 = \langle s_1^{+1} s_0^{-1} \rangle$, $1 = (n, m)$ obtained in our calculations for $J = 0.4t$, $T = 0.005t$, $\eta = 0.05t$ and $t > 0$ (solid lines) and in exact-diagonalization calculations⁵ in a 4×4 lattice for $J = 0.4t$ and $T = 0$ (symbols, dashed lines are drawn as a guide for the eye).

ranges. In spite of the large sensitivity of the spin susceptibility on η , the spin correlations depend only weakly on the hole damping due to the integration over frequencies in the formula for the spin correlations (9). The change of the hole damping from $\eta = 0.05t$ to $0.015t$ leads to the variation in C_1 by several percent.

V. SUMMARY

In this paper the evolution of the hole and spin-excitation spectra of the two-dimensional t - J model was studied in the range of hole concentrations $0 \leq x \lesssim 0.3$

which spans the regions from light to heavy doping. The variation of the spectra with temperature, with the sign of the hopping parameter and with the excitation damping was also considered. For this purpose the self-energy equations were derived employing the projection operator technique and these equations were self-consistently solved. The hole band was found to transform radically at $x \approx 0.08$. A narrow low-concentration band with minima near $(\pm\frac{\pi}{2}, \pm\frac{\pi}{2})$ is converted to a wider band resembling in shape the case of weak electron correlations, with the minimum at (π, π) or at $(0, 0)$ in dependence on the sign of t . The hole Fermi surface is respectively changed from small elliptical pockets at $(\pm\frac{\pi}{2}, \pm\frac{\pi}{2})$ to a large rhombus centered at (π, π) or $(0, 0)$. The frequency dependence of the imaginary part of the magnetic susceptibility χ'' at the antiferromagnetic wave vector depends heavily on the damping of spin excitations and varies from a broad feature similar to that observed¹⁶ in $\text{La}_{2-x}\text{Sr}_x\text{CuO}_4$ to a pronounced maximum which resembles the normal-state resonance peak in $\text{YBa}_2\text{Cu}_3\text{O}_{7-y}$.¹⁷ One of the possible reasons for the variation of the spin-excitation damping is the change of the hole damping. With increasing doping the maximum in the susceptibility loses its intensity and shifts to higher frequencies. The similar behavior is observed in cuprates and is connected with the growth of the spin-excitation frequency at the antiferromagnetic wave vector, which reflects the decrease of the magnetic correlation length with doping.

Acknowledgments

This work was supported by the ESF grant No. 5548.

¹ P. W. Anderson, *Science* **235**, 1196 (1987).
² F. C. Zhang, T. M. Rice, *Phys. Rev. B* **37**, 3759 (1988).
³ Yu. A. Izyumov, *Usp. Fiz. Nauk* **167**, 465 (1997) [*Phys.-Usp. (Russia)* **40**, 445 (1997)]; E. Dagotto, *Rev. Mod. Phys.* **66**, 763 (1994).
⁴ E. Dagotto, R. Joynt, A. Moreo, S. Bacci, E. Gagliano, *Phys. Rev. B* **41**, 9049 (1990).
⁵ J. Bonča, P. Prelovšek, and I. Sega, *Europhys. Lett.* **10**, 87 (1989).
⁶ S.-C. Zhang, J. Carlson, J. E. Gubernatis, *Phys. Rev. B* **55**, 7464 (1997); M. Calandra, S. Sorella, *Phys. Rev. B* **61**, R11894 (2000); S. Sorella, G. B. Martins, F. Becca, C. Gazza, L. Capriotti, A. Parola, E. Dagotto, *Phys. Rev. Lett.* **88**, 117002 (2002).
⁷ S. R. White, D. J. Scalapino, *Phys. Rev. Lett.* **80**, 1272 (1998).
⁸ A. Sherman, M. Schreiber, in *Studies of High Temperature Superconductors*, edited by A. V. Narlikar (Nova Science Publishers, New York, 1999), vol. 27, p. 163; *Physica C* **303**, 257 (1998).
⁹ N. M. Plakida, *Phil. Mag. B* **76**, 771 (1997).
¹⁰ C. L. Kane, P. A. Lee, T. K. Ng, B. Chakraborty, N. Read, *Phys. Rev. B* **41**, 2653 (1990); J. P. Rodriguez, B. Doucot, *Europhys. Lett.* **11**, 451 (1990); X.-G. Wen, P. A. Lee, *Phys. Rev. Lett.* **76**, 503 (1996).
¹¹ A. Damascelli, Z.-X. Shen, and Z. Hussain, *Rev. Mod. Phys.* **75**, 473 (2003).
¹² M. A. Kastner, R. J. Birgeneau, G. Shirane, and Y. Endoh, *Rev. Mod. Phys.* **70**, 897 (1998).
¹³ A. Sherman and M. Schreiber, *Phys. Rev. B* **65**, 134520 (2002); **68**, 094519 (2003); *Eur. Phys. J. B* **32**, 203 (2003).
¹⁴ H. Mori, *Progr. Theor. Phys.* **34**, 399 (1965); A. V. Sherman, *J. Phys. A* **20**, 569 (1987).
¹⁵ A. K. McMahan, J. F. Annett, and R. M. Martin, *Phys. Rev. B* **42**, 6268 (1990); V. A. Gavrichkov, S. G. Ovchinnikov, A. A. Borisov, and E. G. Goryachev, *Zh. Eksp. Teor. Fiz.* **118**, 422 (2000) [*JETP (Russia)* **91**, 369 (2000)].
¹⁶ G. Aeppli, T. E. Mason, S. M. Hayden, H. A. Mook, and J. Kulda, *Science* **279**, 1432 (1997).
¹⁷ P. Bourges, in *The Gap Symmetry and Fluctuations in High Temperature Superconductors*, edited by J. Bok, G. Deutscher, D. Pavuna, and S. A. Wolf (Plenum Press, 1998), p. 349.
¹⁸ J. H. Jefferson, H. Eskes, L. F. Feiner, *Phys. Rev. B* **45**, 7959 (1992); A. V. Sherman, *Phys. Rev. B* **47**, 11521 (1993).

¹⁹ J. Kondo and K. Yamaji, Progr. Theor. Phys. **47**, 807 (1972); H. Shimahara and S. Takada, J. Phys. Soc. Jpn. **61**, 989 (1992); S. Winterfeldt and D. Ihle, Phys. Rev. B **58**, 9402 (1998).

²⁰ A. Sherman and M. Schreiber, Phys. Rev. B **69**, 100505(R) (2004).

²¹ B. Keimer, N. Belk, R. G. Birgeneau, A. Cassanho, C. Y. Chen, M. Greven, M. A. Kastner, A. Aharony, Y. Endoh, R. W. Erwin and G. Shirane, Phys. Rev. B **46**, 14034 (1992).